Journal of Biomechanics 47 (2014) 1767–1776

Contents lists available at ScienceDirect

Journal of Biomechanics

journal homepage: www.elsevier.com/locate/jbiomech
www.JBiomech.com

Microfluidic analysis of red blood cell deformability

Quan Guo [a], Simon P. Duffy [a,b], Kerryn Matthews [a], Aline T. Santoso [a], Mark D. Scott [c,d], Hongshen Ma [a,c,*]

[a] Department of Mechanical Engineering University of British Columbia, 2054-6250 Applied Science Lane, Vancouver, BC, Canada V6T 1Z4
[b] Department of Biology, Kwantlen Polytechnic University, Surrey, BC, Canada
[c] Centre for Blood Research, University of British Columbia, Vancouver, BC, Canada
[d] Department of Pathology and Laboratory Medicine, University of British Columbia, Vancouver, BC, Canada

ARTICLE INFO

Article history:
Accepted 31 March 2014

Keywords:
Cellular biomechanics
Red blood cell
Microfluidics
Cellular deformability

ABSTRACT

A common indicator of rheological dysfunction is a measurable decrease in the deformability of red blood cells (RBCs). Decreased RBC deformability is associated with cellular stress or pathology and can impede the transit of these cells through the microvasculature, where RBCs play a central role in the oxygenation of tissues. Therefore, RBC deformability has been recognized as a sensitive biomarker for rheological disease. In the current study, we present a strategy to measure RBC cortical tension as an indicator of RBC deformability based on the critical pressure required for RBC transit through microscale funnel constrictions. By modeling RBCs as a Newtonian liquid drop, we were able to discriminate cells fixed with glutaraldehyde concentrations that vary as little as 0.001%. When RBCs were sampled from healthy donors on different days, the RBC cortical tension was found to be highly reproducible. Inter-individual variability was similarly reproducible, showing only slightly greater variability, which might reflect biological differences between normal individuals. Both the sensitivity and reproducibility of cortical tension, as an indicator of RBC deformability, make it well-suited for biological and clinical analysis of RBC microrheology.

1. Introduction

The deformability of red blood cells (RBCs) is critical for their transit through the smallest capillaries and is a potent indicator of the health of the cell. Cellular deformability is diminished in RBCs during cellular senescence (Waugh et al., 1992), environmental stress (Antonelou et al., 2010) and micronutrient deficiency (Paterson et al., 1994, 1987; Yip et al., 1983). Furthermore, reduced deformability is common to numerous rheological pathologies, such as malaria parasite blood-stage infection (Glenister et al., 2002; Guo et al., 2012b; Herricks et al., 2009a, 2009b; Hosseini and Feng, 2012; Miller et al., 1972; Mills et al., 2007; Shelby et al., 2003; Suresh et al., 2005), sickle-cell disease (Brandão et al., 2003; Clark et al., 1980; Nash et al., 1984), thalassemia (Advani et al., 1992), elliptocytosis and spherocytosis (Clark et al., 1983; Wandersee et al., 2004). Diminished RBC deformability may be a consequence of disease related cell stress, since reduced RBC deformability can arise from cytoskeletal crosslinking following oxidative stress (Scott et al., 1993, 1992), membrane lipid peroxidation (Dobretsov et al., 1977; Gutteridge, 1995) and vesiculation (Wagner et al., 1987). However, a decrease in RBC deformability may also contribute to the pathology of rheological diseases, as RBCs must undergo significant cell deformation to enter the microvasculature where they play a critical role in respiratory gas exchange. Together, the association between RBC deformability and disease pathology makes the measure of cellular deformability an important biomarker for rheological dysfunction.

The primary challenge associated with measuring cell deformability is that it has a complex rheological property that relies on numerous parameters (cell volume, surface area, cytoplasmic viscosity, and membrane elasticity) (Musielak, 2009). Cell deformability can be inferred from the cellular response to the flow of fluid, such as adsorption or flow rate of the cell suspension through a microfilter (Reid et al., 1976; Worthen et al., 1989) or cell elongation under constant shear stress by rheometry or ektacytometry (Bussolari et al., 1982; Fischer et al., 1978). Filtration strategies are simple to perform but they lack adequate measurement sensitivity while rheometry and ektacytometry have suitable sensitivity for clinical application but are technically difficult to perform and require labor-intensive instrument maintenance between measurements (Groner et al., 1980). Furthermore, both of these strategies only assess the bulk mechanical properties of the cell population and extremely stiff RBC subpopulations may confound measurement of cell deformability.

* Corresponding author at: Department of Mechanical Engineering, University of British Columbia, 2054-6250 Applied Science Lane, Vancouver, BC, Canada V6T 1Z4. Tel.: +1 604 827 4703; fax: +1 604 822 2403.
E-mail address: hongma@mech.ubc.ca (H. Ma).

http://dx.doi.org/10.1016/j.jbiomech.2014.03.038
0021-9290/

Alternatively, the RBC deformability can be accessed from the measurement of single cells. Micropipette aspiration involves partial or complete aspiration of a cell into a glass micropipette and relating the suction pressure to the length of cellular protrusion into the micropipette (Evans and La Celle, 1975; Glenister et al., 2002; Nash et al., 1989; Paulitschke and Nash, 1993). This method measures the shear elastic modulus of the cell membrane, a contributing factor to the deformability of the cell. Another single cell technique, the optical tweezer, uses laser beams to apply a controlled displacement to measure the force-displacement curve between two locations on the RBC membrane (Mills et al., 2007, 2004; Suresh et al., 2005). A third strategy, atomic force microscopy, measures the repulsive force between the surface of a cell and a flexible cantilever (Chen et al., 2009). While single-cell analysis provides precise measurements, these techniques are laborious and only measure the properties of individual cells.

Microfluidic technologies offer the potential for high-throughput single-cell analysis. The most established techniques are adaptations of the cell transit analyzer (CTA) that infers RBC deformability from the time for individual cells to transit micropore structures (Moessmer and Meiselman, 1990). CTA has detected differences in deformability of RBCs from healthy and diseased individuals (Baskurt et al., 1996; Koutsouris et al., 1989; Scott et al., 1993, 1992). Adaptations of this approach measure RBC deformation in capillary obstructions and tapered constrictions (Shelby et al., 2003), transit through constrictions (Gifford et al., 2006, 2003; Herricks et al., 2009a, 2009b), pressure drop while transiting constrictions (Abkarian et al., 2006), and elongation via fluid shear stress (Forsyth et al., 2010; Katsumoto et al., 2010; Lee et al., 2009). Some common limitations of these approaches are that their measures of RBC deformability do not account for variation in cell size, nor do they account for friction between the cell surface and the vessel walls (Zheng et al., 2012).

We present a strategy to infer RBC deformability based on the critical pressure required to deform a RBC through a microscale pore. The RBC may be regarded as a Newtonian liquid drop because it is anucleate and the membrane elasticity, not cytoplasmic viscosity, is the primary determinant of cell deformability (Evans and Hochmuth, 1976). Using the Law of Laplace, we calculate the RBC cortical tension and use this to assess cell deformability. We provide empirical evidence for this simplistic model of a RBC by presenting a microfluidic strategy capable of highly robust and sensitive measurement of RBC cortical tension.

2. Materials and methods

2.1. Sample preparation

Blood was sampled from donors by finger-prick, following informed consent, using a sterile lancet. RBCs were washed in Phosphate Buffered Saline (PBS; $CaCl_2$-free and $MgSO_4$-free; Invitrogen, Carlsbad, CA), by centrifugation 700*g* for 5 min, and diluted to a hematocrit of 0.005 l/l. Washed RBCs were incubated for 30 min (25 °C) with 0–0.003% glutaraldehyde (GA; Alfa Aesar, MA). After incubation, the RBC suspension was washed three times in PBS and resuspended in 0.2% Pluronic™ F-127 (Invitrogen) in PBS, where indicated. Microfluidic analysis was performed immediately.

2.2. Microfluidic device design and operation

The microfluidic device consists of a control layer, that controls valve constriction, and a flow layer, that consists of microchannels and a funnel constriction and was fabricated as described previously (Guo et al., 2012a). The flow channel was pre-incubated for 30 min with a PBS, supplemented with 5% Pluronic™ F-127 and 5% bovine serum albumin (BSA; Sigma-Aldrich, St Louis, MO). The control channels were filled with de-ionized water.

Cells were infused into the flow layer inlet, with valves 1 and 2 closed (Fig. 1A). Narrowing of the microchannel from 200 μm to 50 μm (Fig. 1B) increases the flow speed and spacial resolution between individual cells, such that only one cell transits the funnel region at one time. As the cell enters the constriction region (Fig. 1C), valves 1 and 2 are closed and valves 3 and 4are opened to precisely control

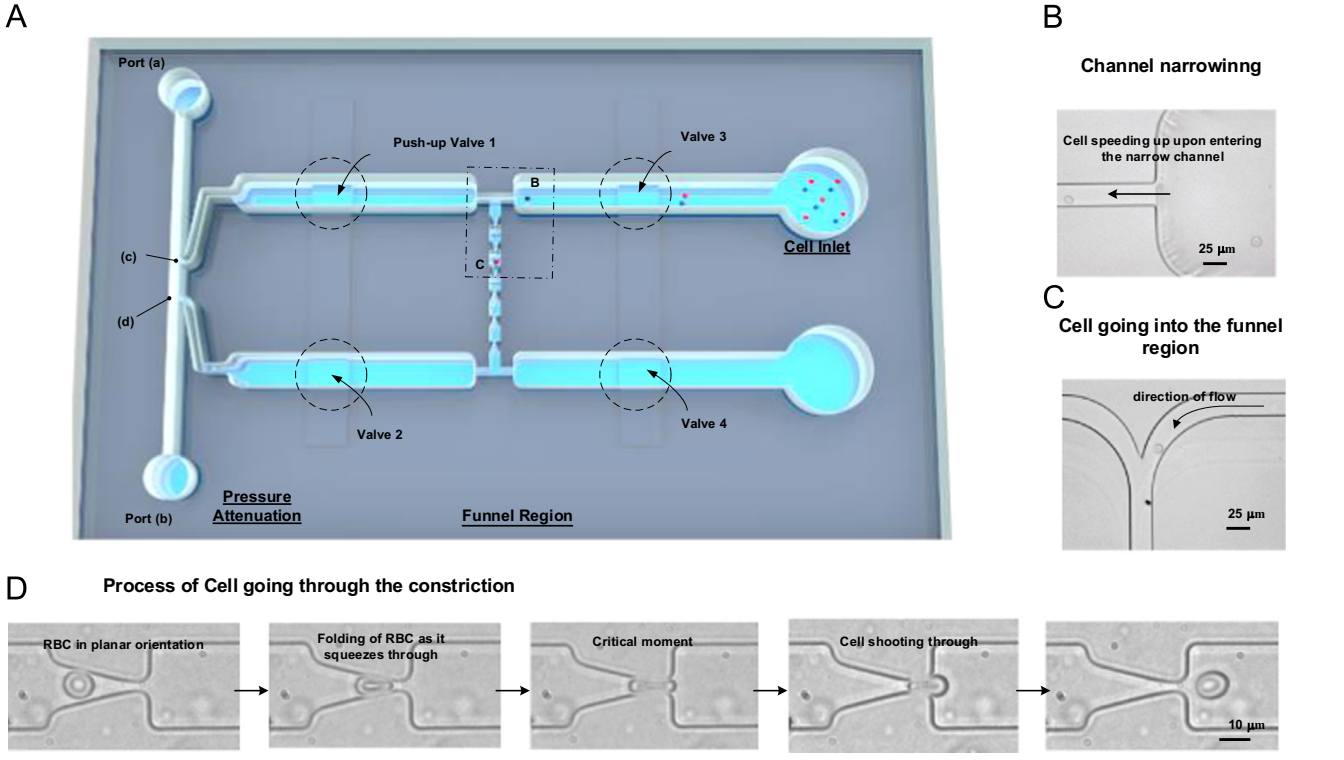

Fig. 1. Design and operation of the microfluidic device for determination of cell deformability. (A) The flow layer of the microfluidic device consists of a pressure attenuator, to precisely control the applied pressure, and a funnel chain, where cell deformation is observed and recorded. Micrographs of cell inlet show that (B) cells accelerate through the narrow channels of the device and (C) are conducted to the funnel chain. (D) Panel of micrographs showing the deformation of a single red blood cell as it passes through the microfluidic funnel.

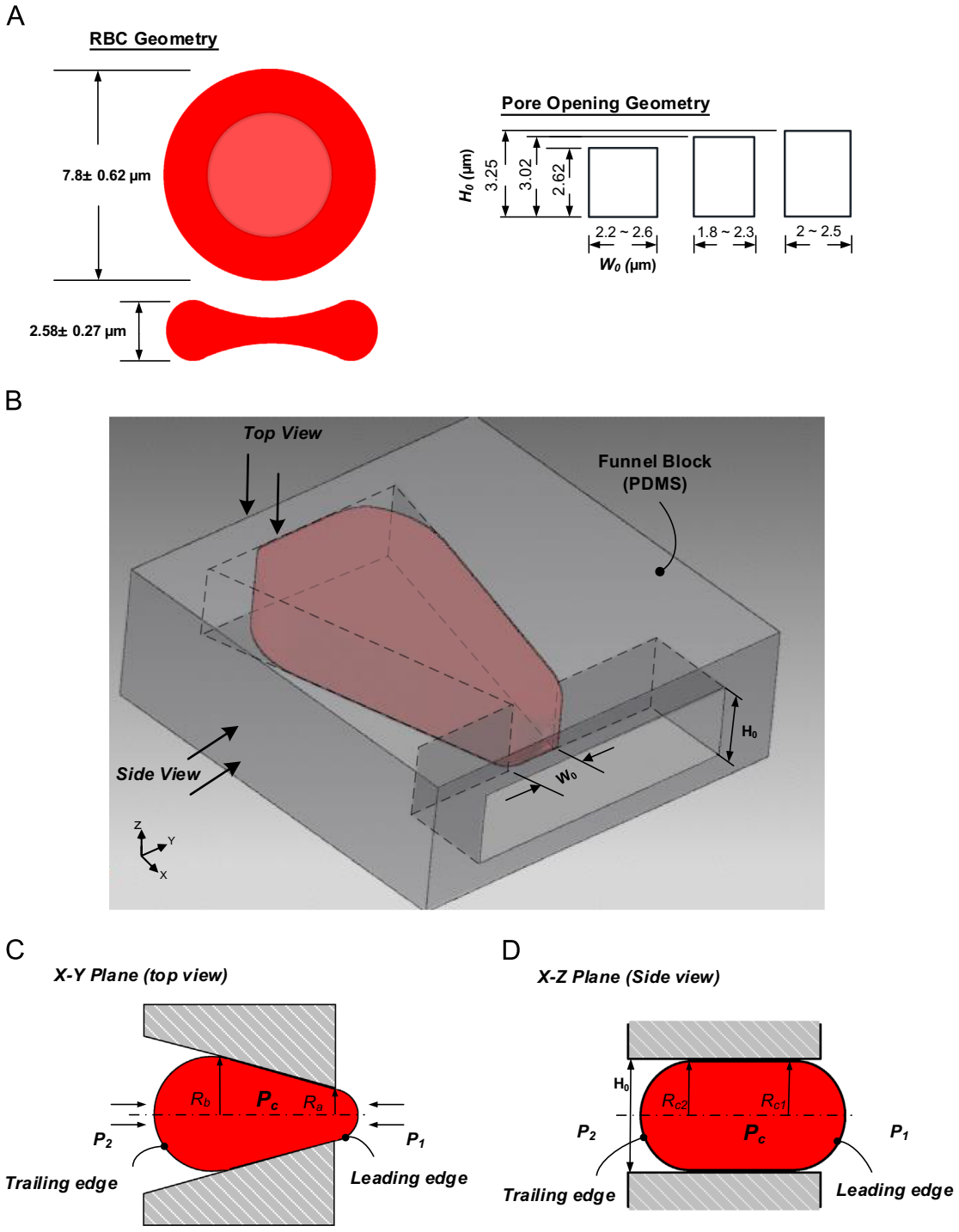

Fig. 2. Geometric representations of both red blood cells (RBCs) and the relevant funnel constrictions used in this analysis. (A) A scale representation of both an RBC and the funnel pore geometries. (B) A 3D plot illustrating the deformation of a RBC through a microscale pore. (C) Top view illustration of a single RBC at the critical point of the funnel constriction (R_a=W$_0$/2); R_a and R_b are the leading and trailing radii formed by the applied pressure difference P_2-P_1 from either end of the cell. (D) Side view of the cell being constricted in the vertical direction with radii R_{C1} and R_{C2} in both leading and trailing edges. P_C indicates the internal pressure of the cell at the critical moment and H_0 denotes the thickness of the funnel.

the applied pressure. The cells enter a funnel with a 30° contraction angle that terminates in microscale pores, sized such that the RBCs obstruct fluid flow must deform during transit (Fig. 2). An externally applied pressure is attenuated using a pressure-divider fluidic circuit, similar to a voltage divider circuit, such that the pressure applied across ports (a) and (b) is divided by a factor of 100 over segments (c) and (d) (Fig. 1A). The applied pressure is increased (0.3 Pa/step) until the cell transits the constriction (Fig. 1D). This threshold pressure was recorded and used to calculate the RBC cortical tension (T_c) using a model of the deformation process. Video microscopy was used to ensure that only a single cell entered the funnel region and to identify the threshold pressure required for funnel transit. For each sample $\geq$40 cells were analyzed and this procedure was performed within 30 min. While the device reported in this study represents a proof-of-principle, we have ongoing efforts to parallelize this device by 90-fold to process ~1000 RBC/h.

2.3. Device geometry measurement

The geometries of the constriction include the vertical height and planar width. The width of the minimum constriction (pore size) is measured by digital microscopy and measurement, using ImageJ, v1.46r (Abramoff et al., 2004). The height of the constriction was measured within 0.1 nm using the Wyko NT1100 (Veeco, Tuscon, AZ) whitelight interferometer.

3. Results and discussion

3.1. Model for evaluating RBC deformability based on threshold pressure

We developed a microfluidic system based on the principles of microfiltration. A precisely controlled applied pressure deforms RBCs (diameter = 7.8 μm; thickness = 2.58 μm) (Kwan et al., 2013) through a funnel pore of defined geometry (Fig. 2A). We hypothesized that RBC deformability may be inferred from the threshold pressure required to transit the pore. This strategy resembles that of CTA (Moessmer and Meiselman, 1990) except that threshold pressure, rather than cell transit time, is used to infer cell deformability. However, we suspected that this measure would be dependent on the geometry of the pore and we generated pores with distinct dimensions to test this hypothesis.

As an alternative strategy we inferred RBC deformability from membrane cortical tension by assuming that the RBC behaves as a Newtonian liquid drop when constricted through a microscale pore. For an intracellular pressure (P_C), P_1 and P_2 are the pressures applied from leading and trailing edges, respectively. R_a and R_b as well as R_{c1} and R_{c2} are the radii of the leading and trailing edges constricted by the width and height of the funnel H_0, respectively (Fig. 2C and D). Using the Laplace Law

$$P_1 - P_c = T_C\left(\frac{1}{R_{c1}} + \frac{1}{R_a}\right) \quad (1)$$

$$P_2 - P_c = T_C\left(\frac{1}{R_{c2}} + \frac{1}{R_b}\right) \quad (2)$$

To find an expression for the applied pressure on the entire cell, we subtract (1) from (2)

$$P_2 - P_1 = T_C\left(\frac{1}{R_a} + \frac{1}{R_{c1}} - \frac{1}{R_b} - \frac{1}{R_{c2}}\right) \quad (3)$$

R_{C1} and R_{C2} are both constrained by the funnel height; therefore these two radii are approximated as being equal. This reduces Eq. (3) to the following final form:

$$P_{threshold} = T_C\left(\frac{1}{R_a} - \frac{1}{R_b}\right) \quad (4)$$

In this model, threshold pressure for cell transit through a constriction depends on the width of the cell (R_a) and funnel pore (R_b), while T_C remains constant. T_C represents the cortical tension of a cell membrane, a property that contributes to the deformability of the cell.

Evans and Yeung proposed that granulocyte cortical tension could be assessed using the Law of Laplace (Evans and Yeung, 1989). This model was replaced by the multi-layered compound drop model on the basis that cells consist of a cytoplasm as well as a 10-fold more viscous nucleoplasm (Dong et al., 1991; Hochmuth et al., 1993).

In contrast with granulocytes, RBCs better resemble a liquid drop because they have no nucleus and the effect of cytoplasmic viscosity on cell deformability is negligible, compared to the membrane cortical tension (Evans and Hochmuth, 1976). Furthermore, while the membrane of granulocytes is highly perforated by microvilli, the surface of RBCs is smooth and the surface-area-to-volume ratio of healthy RBCs deviates by $< 10\%$ (Waugh et al., 1992). Together, the liquid drop model permits a robust measurement of RBC cortical tension that accounts for cell size.

3.2. Minimizing sliding friction

Eq. (4) models the threshold pressure to induce cell transit through a constriction of defined geometry. However, this equation fails to account for the frictional effects of the vessel wall. Sliding friction reduces the transit velocity of cells through the funnel pore (Byun et al., 2013) and this association is non-linear (Preira et al., 2013). Rather than by inducing frictional effects in the existing model, we reduced effects of sliding friction by introducing a lubricating film at the interface between surfaces of both cell and vessel surfaces.

Pluronic™ F127 (Poloxamer 407) has been previously employed to prevent non-specific protein adsorption on the surface of microfluidic systems (Luk et al., 2008). Furthermore, 5% Pluronic™ F127 solutions do not exhibit an inherent cytotoxicity even after 24 h of incubation (Exner et al., 2005). Other studies report that poloxamers do not alter cell shape or size (Hebbel et al., 1987; Karleta et al., 2010). Similarly, we observed no morphological differences among RBCs incubated with Pluronic™ F127. We measured the cortical tension of 584 Pluronic™ F127-treated cells, using 14 chips, and 417 untreated cells, using 10 chips, and observed a lower apparent cortical tension for treated cells, compared to untreated controls (Fig. 3A) as well as reduced the variation in measured cortical tension, compared to untreated controls (Fig. 3B). Together, these data suggest that lubrication of the interface between cell and vessel surfaces diminishes the sliding friction between the two and may facilitate more accurate and sensitive measure of cortical tension.

3.3. Validation of the liquid drop model

An important advantage of determining cortical tension, based on the liquid drop model, is that it accounts for biological variation in RBC size as well as variation in pore geometry, due to limitations associated with microfabrication. We treated RBCs with Pluronic™ F127 and deformed them through microscale pores of varied width (pore size 1.8–2.6 μm) and a height (thickness) that was confined to 2.62 μm, 3.02 μm, and 3.25 μm, respectively

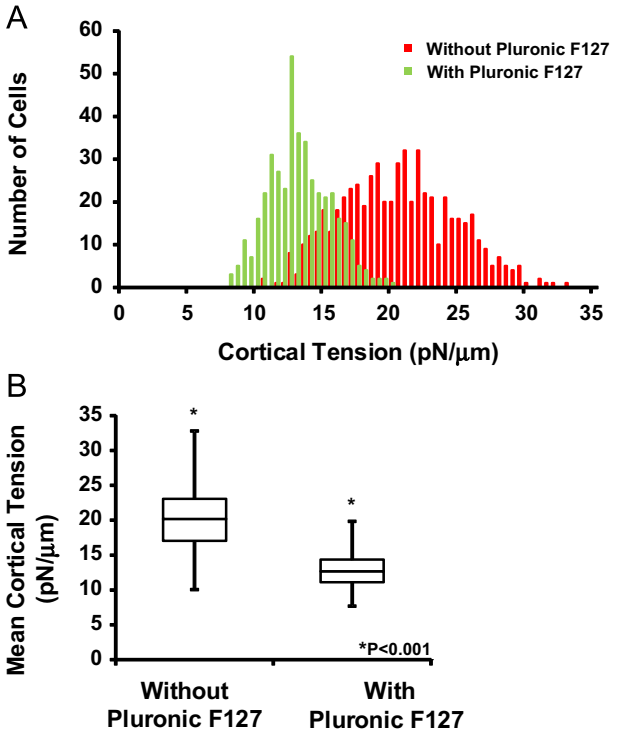

Fig. 3. Measured cortical tension in cells treated with surfactant Pluronic™ F127. (A) Distribution of the number of cells with different measures of cortical tension following treatment with Pluronic™ F127, compared to untreated controls. (B) Box plot representation of mean cellular cortical tension for both Pluronic™ F127 treated cells and untreated controls.

(Fig. 2A). As predicted by the liquid drop model, the mean threshold pressure ($N=40$) was dependent on the constriction geometry and correlated inversely with the constriction width (Fig. 4A; $r^2=0.937$, 0.972 and 0.904, respectively).

In Eq. (4), the threshold pressure depends on the function $(1/R_a-1/R_b)$ and a constant cellular cortical tension (T_C). Correspondingly, the threshold pressure and function $(1/R_a-1/R_b)$ demonstrated a linear relationship (Fig. 4B). At a pore height of 2.62 μm or 3.02 μm there was a strong linear correlation ($r^2=0.943$ and 0.992) and a consistent cortical tension of 10.81 ± 1.75 and 10.60 ± 1.75 pN/μm, respectively. At a pore height of 3.25 μm, the correlation was lower ($r^2=0.837$) and the measured cortical tension was 12.19 ± 2.02 pN/μm (Fig. 4C). A relatively poor relationship between threshold pressure and device geometry for the tallest constriction may represent the geometric limit of the device. We hypothesize that, in a taller constriction, the RBC fails to obstruct fluid flow and greater pressure may be required for the cell to transit the funnel pore, due to fluid leakage, thereby inflating the predicted cortical tension of the cell (Preira et al., 2013). Futhermore, the biconcave shape of RBCs may cause them to fold into "parachute" or "torpedo" shapes (Gregersen et al., 1967; Guest et al., 1963; Skalak and Branemark, 1969) and may also potentially contribute to fluid leakage. Together, these data suggest that the cortical tension of RBCs can be robustly determined using constriction pores ranging from 2.62–3.02 μm in height.

3.4. Intra-individual and inter-individual variability in RBC cortical tension

Intra-individual variability and inter-individual variability in RBC deformability have been extensively investigated by rheometry, ektacytometry and CTA. In healthy individuals, RBC deform-

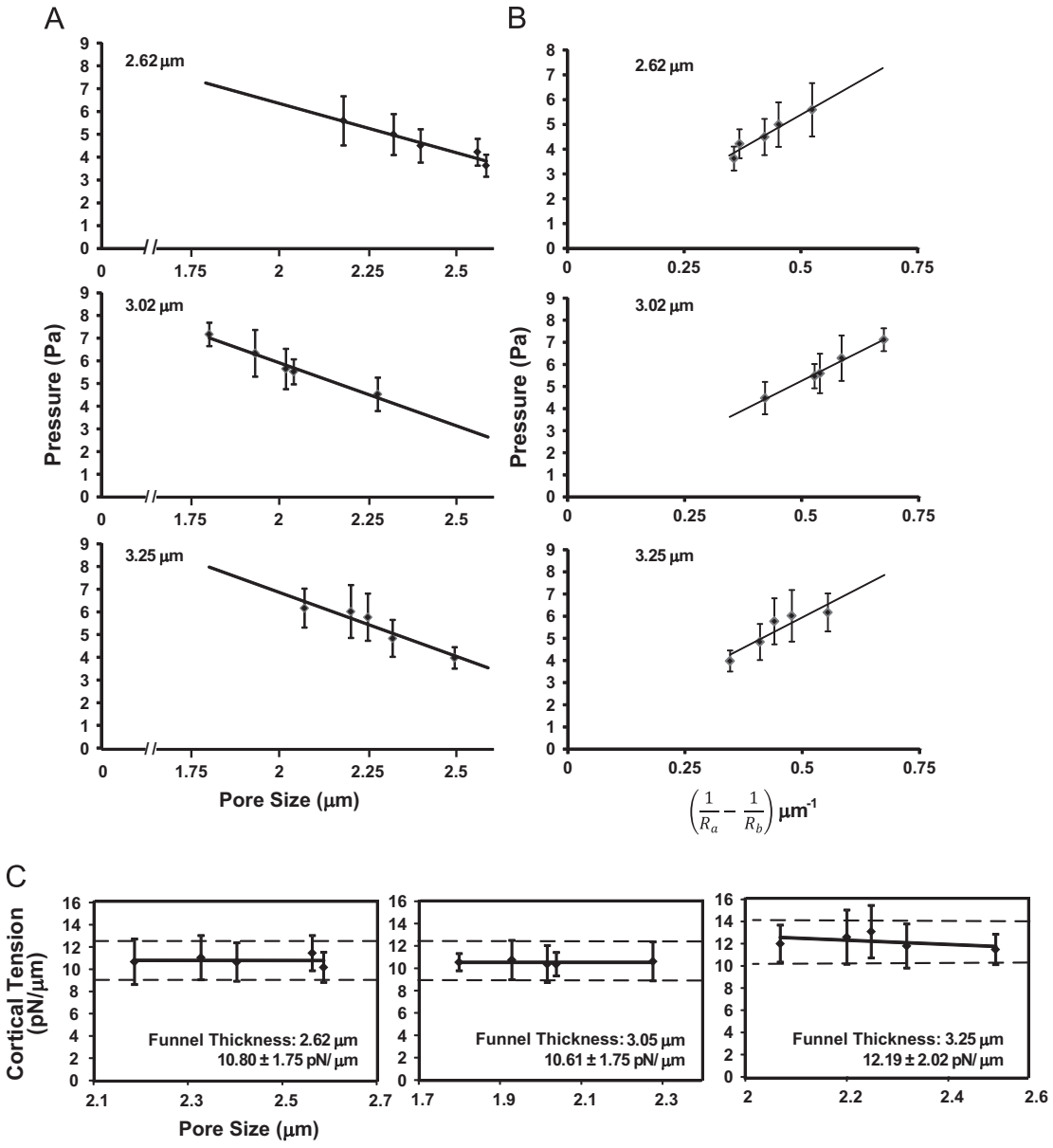

Fig. 4. Examination of pressure and cortical tension as measures of red blood cell (RBC) deformability. (A) The mean threshold pressure required to cause RBCs to transit funnel pores of different geometries. The funnel thickness is indicated on each plot and the pore size is displayed on the *x*-axis. (B) The relationship between the threshold pressure and the function $(1/R_a-1/R_b)$. Based on Laplace law, the cortical tension would represent the slope of each plot. (C) The inferred cortical tension of the RBCs using devices of different geometries. The error bars represent the standard deviation of RBCs for each distinct pore size. The mean cortical tension, inclusive of all pore sizes, is indicated on the plot and the standard deviation is depicted as a dotted line.

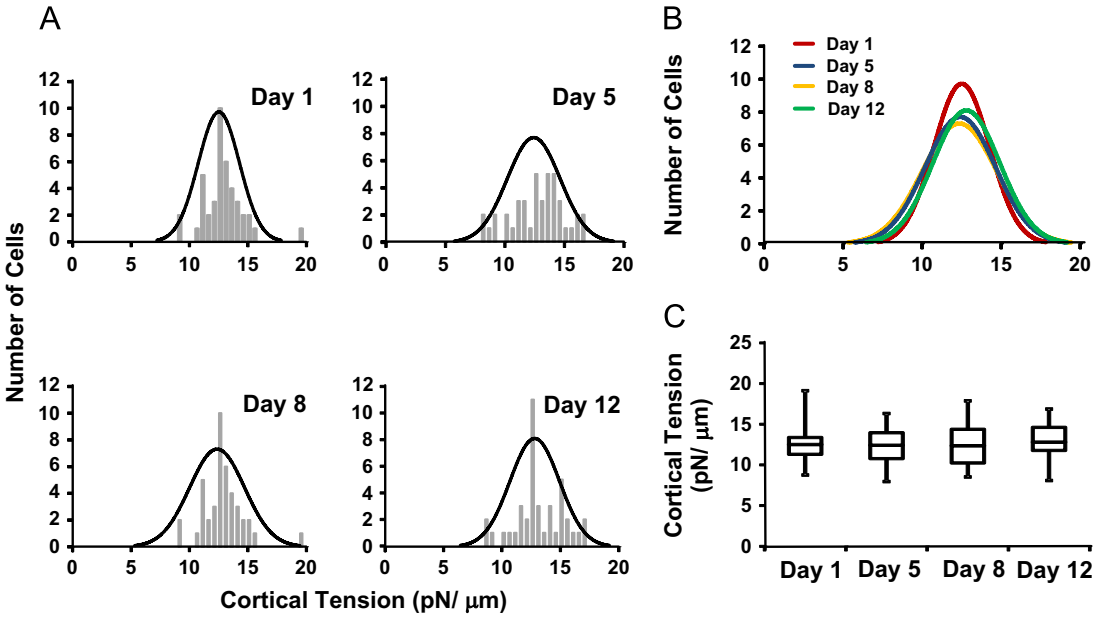

Fig. 5. Intraindividual variation in cortical tensions. (A) Distribution of measured RBC cortical tension from a healthy donor, sampled on four independent days. The black line represents a normal distribution derived from the data. (B) Overlay of the inferred normal distribution of RBC cortical tension for each sample date. (C) Box plot representation of mean cortical tension for each sample date.

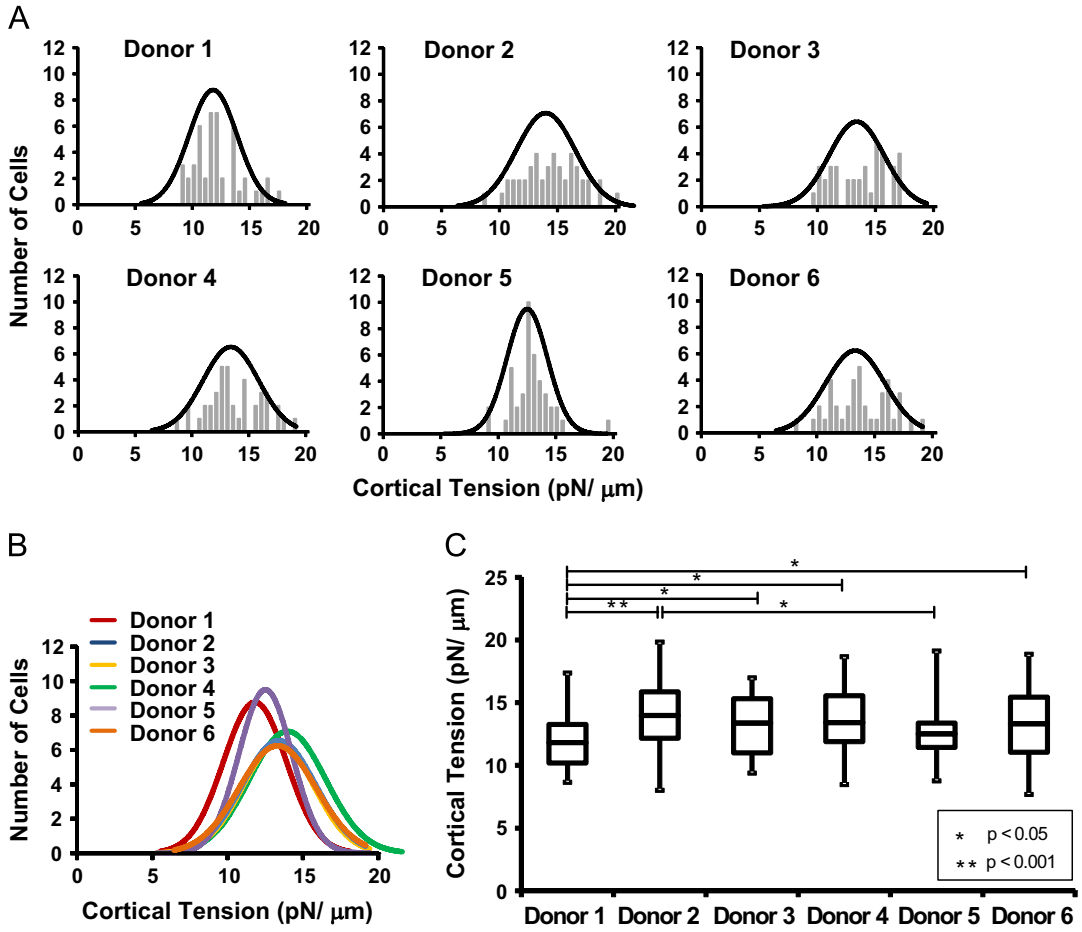

Fig. 6. Variation in RBC cortical tension between individuals. (A) Distribution of measured RBC cortical tension from six healthy donors. The black line represents a normal distribution derived from the data. (B) Overlay of the inferred normal distribution of RBC cortical tension for each sampled individual. (C) Box plot representation of mean cortical tension for each sample date.

ability remains constant over the course of weeks except within 12–24 h of strenuous anaerobic exercise (Kikuchi et al., 1994; Yalcin et al., 2003). However, RBC deformability is subject to natural variability between individuals and can be significantly affected by the age of the individual or pathology (Brun, 2002; El-Sayed et al., 2005; Kikuchi et al., 1994; Yalcin et al., 2003).

Using cortical tension as an indicator of deformability we analyzed the RBCs from a single healthy donor, over 12 days, and also compared the distribution in RBC cortical tension of six healthy donors($N=40$). Consistent with previous reports (Kwan et al., 2013), RBC cortical tension exhibited a distribution value (Fig. 5A) that shows significant overlapping (Fig. 5B). The mean T_C did not vary significantly over the period of analysis, ranging from 12.36–12.80 pN/μm (Fig. 5C). Together, these data demonstrate that mean RBC T_C can be reliably determined over time with a mean coefficient of variance of 1.6%.

In contrast, while T_C measurements from the RBCs six donors also distributed normally (Fig. 6A), the T_C distribution in Donors 1 and 5 was distinct from Donors 2, 3, 4 and 6 (Fig. 6B). Donor 1 displayed a mean T_C that was significantly lower than all other individuals except Donor 5 (Fig. 6C). Donor 5 has the next lowest T_C value but is only significantly lower than the largest value (donor 2). Interestingly, even with this small cohort of healthy donors, significant differences can be observed between the mean T_C of the sampled RBCs.

The consistent intra-individual variability and a low degree of inter-individual variability, in RBC cortical tension is consistent with previous reports (Kikuchi et al., 1994; Yalcin et al., 2003). Kikuchi et al. (1994) reported that a potential limitation of the filtration strategy was its dependence on the hematocrit of the cell suspension, due to clogging of the filter matrix. In contrast, our strategy directly assesses the cortical tension of individual cells in isolation, such that the assessed cell is not affected by the hematocrit of the source suspension. Furthermore, rather than providing only a mean inference for cell deformability, as do the strategies that assess mean elongation and filterability, our strategy generates a profile of RBC cortical tension that would allow assessment of cell subpopulations and deviation from a normal distribution.

3.5. Measurement resolution using mild glutaraldehyde fixation

Glutaraldehyde (GA) fixation induces non-specific dose dependent cross-linking of the cell membrane and has become a standard for comparison of deformability measurement techniques (Baskurt and Meiselman, 2013; Baskurt et al., 2009a; Mirossay et al., 1997). We measured the threshold pressure for GA-treated (0–0.003%; $N=40$) RBCs to transit a 2.62 μm funnel pore. The derived T_C distribution became broader and the mean T_C of the population increased with increasing GA concentration (Fig. 7A). In contrast to untreated cells ($T_C=11.72\pm1.66$ pN/μm), RBCs incubated in as little as 0.0005% GA

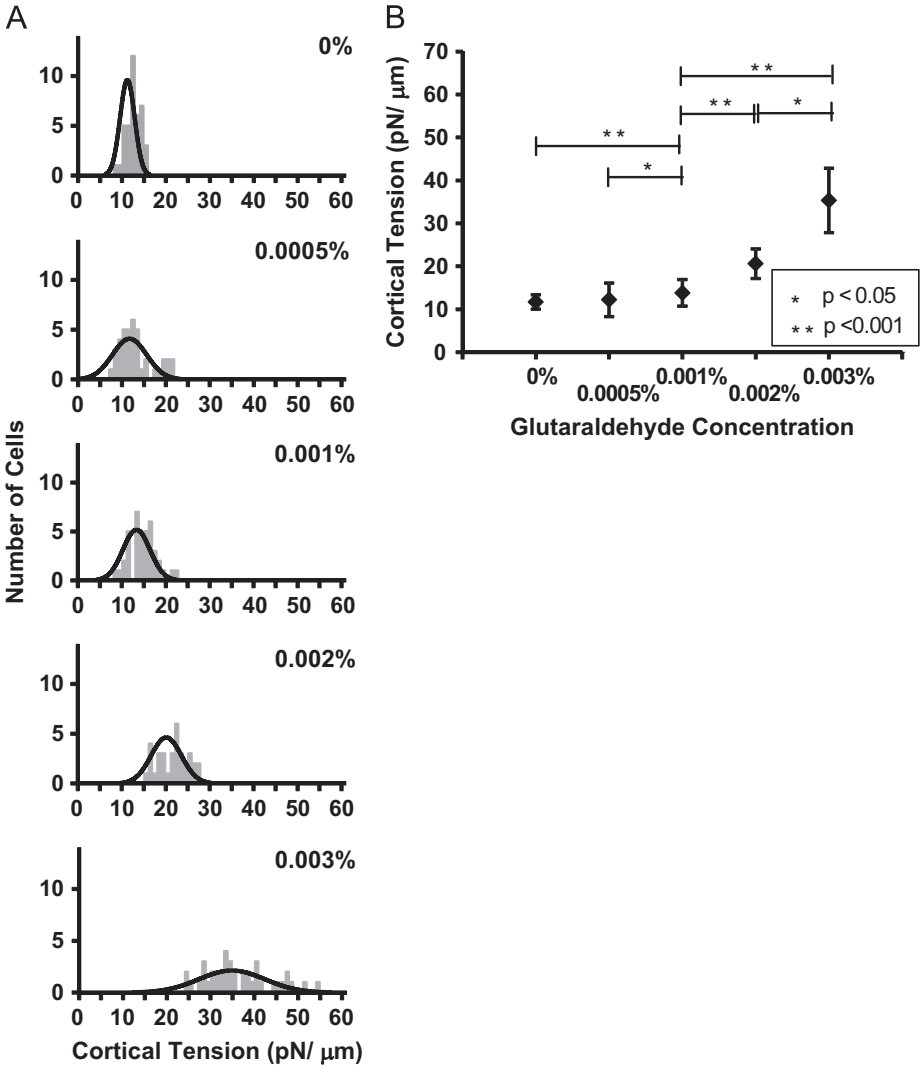

Fig. 7. Cortical tension of RBCs incubated over a range of glutaraldehyde concentrations. (A) Distribution of the number of cells with different measures of cortical tension, at a bin size of 1 pN/μm. The black line represents a normal distribution derived from the data. (B) Population mean of RBCs incubated with different glutaraldehyde concentrations.

Table 1
Comparison of three methods and the percentage inferred increase in cell rigidity, following glutaraldehyde (GA) treatment. Values are normalized against untreated cells.

	Glutaraldehyde concentration					Reference
	0.0005%	0.001%	0.002%	0.003%	0.005%	
Microfluidic funnel	4.20%*	18.04%	75.93%	201.53%	–	Current study
Ektacytometry	–	23.82%	–	57.09%	102.7%	(Baskurt et al., 2009b)**
Cell transit analyzer	–	5.44%	–	9.02%	19.22%	(Baskurt et al., 1996)

* Non-significant increase at $p < 0.05$.
** Based on SS ½ derived from the Lineweaver–Burke method.

Table 2
Comparison of the reproducibility of three techniques for the determination of RBC deformability. The coefficient of variance of measurements derived from the current study, as well as ektacytometry and cell transit analyzer (CTA). The sample size (N) has been included for each study.

	Coefficient of variance		
	Current study	Ektacytometry	CTA
Intra-individual variability	1.56% ($N=4$)	< 5% ($N=10$) (Baskurt et al., 2009a)	2.61% ($N=10$) (Baskurt et al., 1996)
Inter-individual variability	5.90% ($N=6$)	6.24% ($N=5$); (Smith et al., 1999) < 10% ($N=10$) (Baskurt et al., 2009a)	5.05% ($N=10$) (Baskurt et al., 1996)

displayed a non-significant trend toward greater mean cortical tension ($T_C = 12.21 \pm 1.66$ pN/μm; Fig. 7B). A significant difference in mean T_C was observed between all RBC samples incubated in GA concentrations differing by 0.001%.

A valid criticism of our strategy is that the model of an RBC as a liquid drop is overly simplistic. However, the robust and sensitive measurement of GA-induced cytological changes suggests that the measurement of cortical tension represents a phenomenological observation that can yield insight into the deformability of the RBC. While different techniques for assessing RBC deformability examine distinct cytological characteristics we determined that these techniques could be compared based on the relative changes in RBC deformability that they report (Table 1). While CTA is not regarded to be sufficiently precise nor sensitive, below 0.003% GA, for reliable clinical utility (Baskurt et al., 1996), both ektacytometry and our microfluidic strategy can robustly detect significant cytological changes, associated with GA fixation at concentrations as low as 0.001%. Our microfluidic strategy can detect a non-significant 4.2% increase in mean cortical tension, following treatment with 0.0005% GA, and a significant 18.04% increase ($p < 0.05$), when treated with 0.001% GA (Table 1). Due to the laborious nature of micropipette aspiration, there is little information regarding its sensitivity at low GA concentrations. However, it is interesting to note that the elastic shear modulus of intact erythrocytes, treated with 0.005% GA, is 414% greater than untreated cells (Heusinkveld et al., 1977).

We also assessed relatively the reproducibility of microfluidic analysis, ektacytometry and CTA, by determining the coefficient of variance (CoV) for each technique in both intra-individual and inter-individual RBC analysis (Table 2). While all three techniques displayed moderate variation in intra-individual measurement variability, the CoV for inter-individual analyses consistently ranged between 5% and 10%, which may represent biological variation between donors.

Ektacytometry has been well-established as a sensitive technique for assessing RBC deformability and has been accepted as a clinical standard, based on a large number of clinical studies. However, ektacytometry requires the sample to be processed by mixing with a highly viscous solution and is sensitive to variations in the viscosity and electrolyte concentrations of the medium (Mohandas et al., 1980). More importantly, ektacytometry measures only the mean deformability of the RBC population and cannot discriminate cell deformability of RBC subpopulations within the sample. Our microfluidic approach provides a distribution of cortical tension measurements for individual RBCs and is scalable for high-throughput analysis.

4. Conclusions

While RBC deformability has been clinically adopted as a relevant rheological parameter, conventional techniques for the measurement of RBC deformability have the limitations of being technically challenging and providing only an indirect measure of RBC deformability. By modeling RBCs as a Newtonian liquid drop, the current study presents a microfluidic strategy for directly measuring the cortical tension of RBCs. This strategy was shown to be comparable to conventional techniques for RBC deformability measurement in measuring chemically induced as well as biological variation in RBC deformability. This microfluidic strategy permits inference about RBC deformability and may consequently provide valuable information about RBC health and biomechanical characteristics.

Conflict of interest statement

The authors have declared that no competing interests exist.

Acknowledgments

This work was supported by grants from the Canadian Institutes of Health Research (CIHR; Grant no. 259107), Canadian Blood Services (CBS) and Health Canada. The views expressed herein do not necessarily represent the view of the federal government of Canada. We thank the Canada Foundation for Innovation and the Michael Smith Foundation for Health Research for infrastructure funding at the University of British Columbia Centre for Blood Research. Study sponsors did not contribute to the study design or in the collection, analysis and interpretation of data. Study sponsors did not influence the writing of the manuscript or the decision to submit the manuscript for publication.

References

Abkarian, M., Faivre, M., Stone, H.a., 2006. High-speed microfluidic differential manometer for cellular-scale hydrodynamics. Proc. Natl. Acad. Sci. USA 103, 538–542.

Abramoff, M., Magalhaes, P., Ram, S., 2004. Image processing with ImageJ. Biophotonics Int. 11, 36–42.

Advani, R., Rubin, E., Mohandas, N., Schrier, S.L., 1992. Oxidative red blood cell membrane injury in the pathophysiology of severe mouse beta-thalassemia. Blood 79, 1064–1067.

Antonelou, M.H., Kriebardis, A.G., Papassideri, I.S., 2010. Aging and death signalling in mature red cells: from basic science to transfusion practice. Blood Transfus. Trasfus. Sangue 8 (Suppl. 3), s39–s47.

Baskurt, O.K., Fisher, T.C., Meiselman, H.J., 1996. Sensitivity of the cell transit analyzer (CTA) to alterations of red blood cell deformability: role of cell size-pore size ratio and sample preparation. Clin. Hemorheol. 16, 753–765.

Baskurt, O.K., Hardeman, M.R., Uyuklu, M., Ulker, P., Cengiz, M., Nemeth, N., Shin, S., Alexy, T., Meiselman, H.J., 2009a. Comparison of three commercially available ektacytometers with different shearing geometries. Biorheology 46, 251–264.

Baskurt, O.K., Hardeman, M.R., Uyuklu, M., Ulker, P., Cengiz, M., Nemeth, N., Shin, S., Alexy, T., Meiselman, H.J., 2009b. Parameterization of red blood cell elongation index-shear stress curves obtained by ektacytometry. Scand. J. Clin. Lab. Investig. 69, 777–788.

Baskurt, O.K., Meiselman, H.J., 2013. Data reduction methods for ektacytometry in clinical hemorheology. Clin. Hemorheol. Microcirc. 54, 99–107.

Brandão, M.M., Fontes, A., Barjas-Castro, M.L., Barbosa, L.C., Costa, F.F., Cesar, C.L., Saad, S.T.O., Brandao, M.M., 2003. Optical tweezers for measuring red blood cell elasticity: application to the study of drug response in sickle cell disease. Eur. J. Haematol. 70, 207–211.

Brun, J.-F., 2002. Exercise hemorheology as a three acts play with metabolic actors: is it of clinical relevance? Clin. Hemorheol. Microcirc. 26, 155–174.

Bussolari, S.R., Dewey Jr, C.F., Gimbrone Jr, M.A., 1982. Apparatus for subjecting living cells to fluid shear stress. Rev. Sci. Instrum. 53, 1851–1854.

Byun, S., Son, S., Amodei, D., Cermak, N., Shaw, J., Kang, J.H., Hecht, V.C., Winslow, M.M., Jacks, T., Mallick, P., et al., 2013. Characterizing deformability and surface friction of cancer cells. Proc. Natl. Acad. Sci. USA 110, 7580–7585.

Chen, X., Feng, L., Jin, H., Feng, S., Yu, Y., 2009. Quantification of the erythrocyte deformability using atomic force microscopy: correlation study of the erythrocyte deformability with atomic force microscopy and hemorheology. Clin. Hemorheol. Microcirc. 43, 243–251.

Clark, M.R., Mohandas, N., Shohet, S.B., 1980. Deformability of oxygenated irreversibly sickled cells. J. Clin. Invest. 65, 189–196.

Clark, M.R., Mohandas, N., Shohet, S.B., 1983. Osmotic gradient ektacytometry: comprehensive characterization of red cell volume and surface maintenance. Blood 61, 899–910.

Dobretsov, G.E., Borschevskaya, T.A., Petrov, V.A., Vladimirov, Y.A., 1977. The increase of phospholipid bilayer rigidity after lipid peroxidation. FEBS Lett. 84, 125–128.

Dong, C., Skalak, R., Sung, K.L., 1991. Cytoplasmic rheology of passive neutrophils. Biorheology 28, 557–567.

El-Sayed, M.S., Ali, N., El-Sayed Ali, Z., 2005. Haemorheology in exercise and training. Sports Med. 35, 649–670.

Evans, E.A., Hochmuth, R.M., 1976. Membrane viscoelasticity. Biophys. J. 16, 1–11.

Evans, E.A., La Celle, P.L., 1975. Intrinsic material properties of the erythrocyte membrane indicated by mechanical analysis of deformation. Blood 45, 29–43.

Evans, E.A., Yeung, A., 1989. Apparent viscosity and cortical tension of blood granulocytes determined by micropipet aspiration. Biophys. J. 56, 151–160.

Exner, A.A., Krupka, T.M., Scherrer, K., Teets, J.M., 2005. Enhancement of carboplatin toxicity by pluronic block copolymers. J. Control. Release 106, 188–197.

Fischer, T.M., Stohr-Lissen, M., Schmid-Schonbein, H., 1978. The red cell as a fluid droplet: tank tread-like motion of the human erythrocyte membrane in shear flow. Science 202, 894–896.

Forsyth, A.M., Wan, J., Ristenpart, W.D., Stone, H.a., 2010. The dynamic behavior of chemically "stiffened" red blood cells in microchannel flows. Microvasc. Res. 80, 37–43.

Gifford, S.C., Derganc, J., Shevkoplyas, S.S., Yoshida, T., Bitensky, M.W., 2006. A detailed study of time-dependent changes in human red blood cells: from reticulocyte maturation to erythrocyte senescence. Br. J. Haematol. 135, 395–404.

Gifford, S.C., Frank, M.G., Derganc, J., Gabel, C., Austin, R.H., Yoshida, T., Bitensky, M.W., 2003. Parallel microchannel-based measurements of individual erythrocyte areas and volumes. Biophys. J. 84, 623–633.

Glenister, F.K., Coppel, R.L., Cowman, A.F., Mohandas, N., Cooke, B.M., 2002. Contribution of parasite proteins to altered mechanical properties of malaria-infected red blood cells. Blood 99, 1060–1063.

Gregersen, M.I., Bryant, C.A., Hammerle, W.E., Usami, S., Chien, S., 1967. Flow characteristics of human erythrocytes through polycarbonate sieves. Science 157, 825–827.

Groner, W., Mohandas, N., Bessis, M., 1980. New optical technique for measuring erythrocyte deformability with the ektacytometer. Clin. Chem. 26, 1435–1442.

Guest, M.M., Bond, T.P., Cooper, R.G., Derrick, J.R., 1963. Red blood cells: change in shape in capillaries. Science 142, 1319–1321.

Guo, Q., Park, S., Ma, H., 2012a. Microfluidic micropipette aspiration for measuring the deformability of single cells. Lab Chip 12, 2687–2695.

Guo, Q., Reiling, S.J., Rohrbach, P., Ma, H., 2012b. Microfluidic biomechanical assay for red blood cells parasitized by *Plasmodium falciparum*. Lab Chip 12, 1143–1150.

Gutteridge, J.M., 1995. Lipid peroxidation and antioxidants as biomarkers of tissue damage. Clin. Chem. 41, 1819–1828.

Hebbel, R., Tukey, D., Clawson, C., White, J., Vercellotti, G., et al., 1987. Pluronic F-68 reduces the endothelial adherence and improves the rheology of liganded sickle erythrocytes. Blood 69, 1631–1636.

Herricks, T, Antia, M., Rathod, P.K., 2009a. Deformability limits of *Plasmodium falciparum*-infected red blood cells. Cell. Microbiol. 11, 1340–1353.

Herricks, Thurston, Antia, M., Rathod, P.K., 2009b. Deformability limits of *Plasmodium falciparum*–infected red blood cells. Cell. Microbiol. 11, 1340–1353.

Heusinkveld, R.S., Goldstein, D.A., Weed, R.I., La Celle, P.L., 1977. Effect of protein modification on erythrocyte membrane mechanical properties. Blood Cells 3, 175.

Hochmuth, R.M., Ting-Beall, H.P., Beaty, B.B., Needham, D., Tran-Son-Tay, R., 1993. Viscosity of passive human neutrophils undergoing small deformations. Biophys. J. 64, 1596–1601.

Hosseini, S.M., Feng, J.J., 2012. How malaria parasites reduce the deformability of infected red blood cells. Biophys. J. 103, 1–10.

Karleta, V., Andrlik, I., Braunmüller, S., Franke, T., Wirth, M., Gabor, F., 2010. Poloxamer 188 supplemented culture medium increases the vitality of Caco-2 cells after subcultivation and freeze/thaw cycles. Altex 27, 191.

Katsumoto, Y., Tatsumi, K., Doi, T., Nakabe, K., 2010. Electrical classification of single red blood cell deformability in high-shear microchannel flows. Int. J. Heat Fluid Flow 31, 985–995.

Kikuchi, Y., Da, Q.W., Fujino, T., 1994. Variation in red blood cell deformability and possible consequences for oxygen transport to tissue. Microvasc. Res. 47, 222–231.

Koutsouris, D., Guillet, R., Wenby, R.B., Meiselman, H.J., 1989. Determination of erythrocyte transit times through micropores. II. Influence of experimental and physicochemical factors. Biorheology 26, 881–898.

Kwan, J.M., Guo, Q., Kyluik-Price, D.L., Ma, H., Scott, M.D., 2013. Microfluidic analysis of cellular deformability of normal and oxidatively damaged red blood cells. Am. J. Hematol. 88, 682–689.

Lee, S.S., Yim, Y., Ahn, K.H., Lee, S.J., 2009. Extensional flow-based assessment of red blood cell deformability using hyperbolic converging microchannel. Biomed. Microdevices 11, 1021–1027.

Luk, V.N., Mo, G.C., Wheeler, A.R., 2008. Pluronic additives: a solution to sticky problems in digital microfluidics. Langmuir ACS J. Surf. Colloids 24, 6382–6389.

Miller, L.H., Usami, S., Chien, S., 1972. Decreased deformability of Plasmodium-coatneyi-infected red-cells and its possible relation to cerebral malaria. Am. J. Trop. Med. Hyg. 21, 133–137.

Mills, J.P., Diez-Silva, M., Quinn, D.J., Dao, M., Lang, M.J., Tan, K.S.W., Lim, C.T., Milon, G., David, P.H., Mercereau-Puijalon, O., Bonnefoy, S., Suresh, S., 2007. Effect of plasmodial RESA protein on deformability of human red blood cells harboring *Plasmodium falciparum*. Proc. Natl. Acad. Sci. USA 104, 9213–9217.

Mills, J.P., Qie, L., Dao, M., Tan, K.S.W., Lim, C.T., Suresh, S., 2004. Continuous force-displacement relationships for the human red blood cell at different erythrocytic developmental stages of *Plasmodium falciparum* malaria parasite. MRS Proc., 844.

Mirossay, L., Mojzis, J., Jandoseková, M., Lukacín, S., Nicák, A., 1997. Comparison of two methods in erythrocyte microrheology determination using glutaraldehyde-treated cells. Clin. Hemorheol. Microcirc. 17, 187–192.

Moessmer, G., Meiselman, H.J., 1990. A new micropore filtration approach to the analysis of white cell rheology. Biorheology 27, 829–848.

Mohandas, N., Clark, M.R., Jacobs, M.S., Shohet, S.B., 1980. Analysis of factors regulating erythrocyte deformability. J. Clin. Invest. 66, 563–573.

Musielak, M., 2009. Red blood cell-deformability measurement: review of techniques. Clin. Hemorheol. Microcirc. 42, 47–64.

Nash, G.B., Johnson, C.S., Meiselman, H.J., 1984. Mechanical properties of oxygenated red blood cells in sickle cell (HbSS) disease. Blood 63, 73–82.

Nash, G.B., O'Brien, E., Gordon-Smith, E.C., Dormandy, J.A., 1989. Abnormalities in the mechanical properties of red blood cells caused by *Plasmodium falciparum*. Blood 74, 855–861.

Paterson, P.G., Allen, O.B., Bettger, W.J., 1987. Effect of dietary zinc deficiency on the endogenous phosphorylation and dephosphorylation of rat erythrocyte membrane. J. Nutr. 117, 2096–2105.

Paterson, P.G., Gorecki, D.K., Card, R.T., 1994. Vitamin E deficiency and erythrocyte deformability in the rat. J. Nutr. Biochem. 5, 298–302.

Paulitschke, M., Nash, G.B., 1993. Membrane rigidity of red blood cells parasitized by different strains of *Plasmodium falciparum*. J. Lab. Clin. Med. 122, 581–589.

Preira, P., Valignat, M.-P., Bico, J., Théodoly, O., 2013. Single cell rheometry with a microfluidic constriction: quantitative control of friction and fluid leaks between cell and channel walls. Biomicrofluidics 7, 024111.

Reid, H.L., Barnes, A.J., Lock, P.J., Dormandy, J.A., Dormandy, T.L., 1976. Simple method for measuring erythrocyte deformability. J. Clin. Pathol. 29, 855–858.

Scott, M.D., Rouyer-Fessard, P., Ba, M.S., Lubin, B.H., Beuzard, Y., 1992. α- and β-haemoglobin chain induced changes in normal erythrocyte deformability: comparison to β thalassaemia intermedia and Hb H disease. Br. J. Haematol. 80, 519–526.

Scott, M.D., van den Berg, J.J., Repka, T., Rouyer-Fessard, P., Hebbel, R.P., Beuzard, Y., Lubin, B.H., 1993. Effect of excess alpha-hemoglobin chains on cellular and membrane oxidation in model beta-thalassemic erythrocytes. J. Clin. Invest. 91, 1706–1712.

Shelby, J.P., White, J., Ganesan, K., Rathod, P.K., Chiu, D.T., 2003. A microfluidic model for single-cell capillary obstruction by *Plasmodium falciparum* infected erythrocytes. Proc. Natl. Acad. Sci. USA 100, 14618–14622.

Skalak, R., Branemark, P.I., 1969. Deformation of red blood cells in capillaries. Science 164, 717–719.

Smith, J.A., Martin, D.T., Telford, R.D., Ballas, S.K., 1999. Greater erythrocyte deformability in world-class endurance athletes. Am. J. Physiol. 276, H2188–H2193.

Suresh, S., Spatz, J., Mills, J.P., Micoulet, A., Dao, M., Lim, C.T., Beil, M., Seufferlein, T., 2005. Connections between single-cell biomechanics and human disease states: gastrointestinal cancer and malaria. Acta Biomater. 1, 15–30.

Wagner, G.M., Chiu, D.T., Qju, J.H., Heath, R.H., Lubin, B.H., 1987. Spectrin oxidation correlates with membrane vesiculation in stored RBCs. Blood 69, 1777–1781.

Wandersee, N.J., Olson, S.C., Holzhauer, S.L., Hoffmann, R.G., Barker, J.E., Hillery, C.A., 2004. Increased erythrocyte adhesion in mice and humans with hereditary spherocytosis and hereditary elliptocytosis. Blood 103, 710–716.

Waugh, R.E., Narla, M., Jackson, C.W., Mueller, T.J., Suzuki, T., Dale, G.L., 1992. Rheologic properties of senescent erythrocytes: loss of surface area and volume with red blood cell age. Blood 79, 1351–1358.

Worthen, G.S., Schwab 3rd, B., Elson, E.L., Downey, G.P., 1989. Mechanics of stimulated neutrophils: cell stiffening induces retention in capillaries. Science 245, 183–186.

Yalcin, O., Erman, A., Muratli, S., Bor-Kucukatay, M., Baskurt, O.K., 2003. Time course of hemorheological alterations after heavy anaerobic exercise in untrained human subjects. J. Appl. Physiol. 1985 (94), 997–1002.

Yip, R., Mohandas, N., Clark, M.R., Jain, S., Shohet, S.B., Dallman, P.R., 1983. Red cell membrane stiffness in iron deficiency. Blood 62, 99–106.

Zheng, Y., Shojaei-Baghini, E., Azad, A., Wang, C., Sun, Y., 2012. High-throughput biophysical measurement of human red blood cells. Lab Chip 12, 2560–2567.